Progress In Electromagnetics Research C, Vol. 48, 141–150, 2014

Design of H-Plane Inductance Diaphragm Waveguide Band-Pass Filter for Millimeter Imaging Frontend

Baohua Yang, Zhiping Li*, Jin Zhang, Xianxun Yao, Cheng Zheng, Xiaozhou Shang, and Jungang Miao

Abstract—This study presents an equivalent circuit and a design of an H-plane waveguide bandpass filter (BPF) with chamfer. Traditionally, only thin inductive diaphragm with no chamfers considered in the direct-coupled cavity theory, but this will lead to difficulties in the BPF manufacturing. During manufacturing process the chamfer cannot be avoided, and its equivalent circuit and effects on frequency shifting are investigated in this paper. A new design method is proposed in order to compensate the effect of chamfer in the half-wavelength resonator connection between the inductance diaphragm and the waveguide. A modified empirical formula and corresponding procedure are provided for designing such filters. The working center frequency and 3 dB bandwidths (BW) are simulated considering different chamfer radius. The simulated center frequencies are 18 GHz, 26 GHz, 34 GHz and 42 GHz, and BWs are 2.265%, 2.5%, 10%, 15% and 20%. Results show that the modified formula, which conforms better with the simulated results, is superior to the traditional formula. Two H-plane waveguide BPFs are manufactured with center frequency 26 GHz with 2.5% BW and 34 GHz with 2.265% BW. The results of the modified formula are in good agreement with measured ones.

1. INTRODUCTION

As millimeter wave (MMW) electronic technology develops, the passive MMW imaging technique is used for human body security inspection, which is becoming an effective approach to detect dangerous objects under the clothes, such as concealed weapons or plastic explosive [1–3]. Various passive MMW imaging systems have been developed by the Electromagnetic Laboratory of Beihang University [4–9].

In order to achieve high level of integration and compact dimension, their MMW receiver front-ends are realized using MMICs while the passive components such as BPF are often realized off-chip [8], and in turn achieve high imaging resolution. The BPF are used in the radio frequency receivers for image frequency rejection outside the image frequency which results in improved sensitivity. The BPF is realised by waveguide which has many advantages such as high rejection of image frequency, high Q value, low insertion loss, good temperature stability, easy design, easy manufacturing and installation [10]. In the design of direct coupling waveguide BPF the inductive diaphragms, pins or E insert are commonly used as coupling network between levels of waveguide resonant cavity [11, 12]. Only one similar H-plane waveguide BPF is reported [13]. However, the filter is sensitive to the length of resonators, and in the process of manufacture when the milling cutter is used the round chamfer is unavoidable, and the effect is the changing of active resonators' effective lengths, thus the center frequency. In this paper, a novel design method of H-plane waveguide BPF has been proposed and realised which accounts for this chamfer effect and possesses flexible tuning ability.

In this paper, the design procedure of a rectangular waveguide BPF using H-plane inductive diaphragm with round chamfer is presented. An empirical solution is found which aims at the frequency

Received 14 January 2014, Accepted 16 March 2014, Scheduled 21 March 2014

* Corresponding author: Zhiping Li (zhiping_li@buaa.edu.cn).

The authors are with the School of Electronic Information and Engineering, Beihang University, Beijing 100191, China.

shifting caused by round chamfer. Five waveguide BPFs with center frequencies of 18 GHz, 26 GHz, 34 GHz and 42 GHz and relative 3 dB BWs of 2.265%, 25.%, 10%, 15% and 20% are simulated to investigate the frequency shifting. Only 26 GHz and 34 GHz filters are manufactured and measured. The measured results are in good agreement with the simulated ones after chamfer compensation and thru, reflect and line calibration method (TRL) [8]. The design procedure and frequency shifting lines are discussed in Section 2. The measured results are described in Section 3 followed by conclusions.

2. DESIGN ANALYSIS

The top view and 3D view of the H-plane waveguide BPF are shown in Figs. 1(a) and (b), respectively, the half wavelength waveguide sections are used as series resonators, the parallel inductance diaphragms are used as coupling structure between the resonators. Fig. 1(c) shows the unavoidable round chamfer during actual manufacture. Fig. 2 shows the equivalent circuit of the inserted metal diaphragm of H-plane waveguide BPF. The design procedure is proposed as follows.

(a) Top view (b) 3D view (c) 3D view with chamfer

Figure 1. The structure of H-plane waveguide BPF, (a) top view, (b) 3D view, (c) 3D view with chamfer.

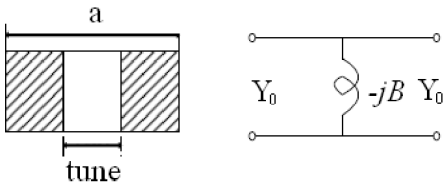

(a) Diaphragm (b) The equivalent circuit

Figure 2. The inserted inductance diaphragm and its T type equivalent circuit, (a) diaphragm, (b) the equivalent circuit.

For the large scale application of filters in passive MMW systems, the accurate characterization of the filter frequency response and the reproducibility of the filters are the primary concern. The procedure and formula for the design of H-plane waveguide BPF are reported in the literature [14].

In order to analyse the waveguide filter character, the inserted metal diaphragm in the waveguide is equivalent to a T-type reactance network shown in Fig. 2 [11].

According to Formulae (1) to (3), the transformation of low-pass and band-pass can be realized only for TE_{10} mode transmission in this type of waveguide filter. Formula (1) is the approximation transformation between the low-pass filter and pass-band filter.

$$\frac{\omega'}{\omega'_1} = \frac{2}{w_\lambda}\left(\frac{\lambda_{g0} - \lambda_g}{\lambda_{g0}}\right) \tag{1}$$

$$w_\lambda = \frac{\lambda_{g1} - \lambda_{g2}}{\lambda_{g0}} = \left(\frac{\lambda_{g0}}{\lambda_0}\right)^2 \left(\frac{\omega_2 - \omega_1}{\omega_0}\right) \tag{2}$$

$$\lambda_{g0} = \frac{\lambda_{g1} + \lambda_{g2}}{2} \tag{3}$$

ω', ω'_1 are the frequency variable and band-edge frequency of the prototype low-pass filter respectively, and λ_{g0}, λ_{g1}, λ_{g2}, λ_g are the waveguide wavelengths corresponding to the frequencies ω_0, ω_1, ω_2 and ω

of BPF, respectively. ω is frequency variable, ω_0 the center frequency, and ω_1 and ω_2 are the band-edge frequencies. w_λ is the relative bandwidth, X_j reactance slope parameters of the resonator series, and Z_0 the characteristic impedance 50 ohm.

$$X_j = \frac{\pi}{2} Z_0 \left(\frac{\lambda_{g0}}{\lambda_0}\right)^2 \tag{4}$$

Substitute X_j into the impedance transformation formula (5) to (7).

$$K_{01} = \sqrt{\frac{R_A X_1 \omega}{g_0 g_1 \omega_1'}} \tag{5}$$

$$K_{j,j+1}|_{j=1\to n-1} = \frac{\omega}{\omega_1'} \sqrt{\frac{X_j X_{j+1}}{g_j g_{j+1}}} \tag{6}$$

$$K_{n.n+1} = \sqrt{\frac{R_S X_n \omega}{g_n g_{n+1} \omega_1'}} \tag{7}$$

The impedance transformation formula of waveguide filter can be obtained applying (8) to (10) [15].

$$\frac{K_{01}}{Z_0} = \sqrt{\frac{\pi w_\lambda}{2 g_0 g_1 \omega_1'}} \tag{8}$$

$$\frac{K_{j,j+1}}{Z_0}|_{j=1\to n-1} = \frac{\pi w_\lambda}{2\omega_1'} \frac{1}{\sqrt{g_j g_{j+1}}} \tag{9}$$

$$\frac{K_{n,n+1}}{Z_0} = \sqrt{\frac{\pi w_\lambda}{2 g_n g_{n+1} \omega_1'}} \tag{10}$$

K is a function of frequency named impedance of the converter and g the parameters of the Chebyshev low-pass filter. The section of the inductive BPF is shown in Fig. 3, and the equivalent inductors are separated by electrical length θ. The impedance converter of Fig. 3 consists of a shunt inductance jX at the center of a short length of transmission line of electrical length ϕ, and the impedance converter is given by Levy [15]. The transfer matrix of an ideal impedance converter is given.

$$\begin{bmatrix} 0 & \pm jK \\ \pm j/K & 0 \end{bmatrix} \tag{11}$$

The transfer matrix of the actual impedance converter of Fig. 2(b) is

$$\begin{bmatrix} A & B \\ C & D \end{bmatrix} = \begin{bmatrix} \cos\phi - \dfrac{\sin\phi}{2X/Z_0} & -j\left(\sin\phi + \dfrac{\cos\phi - 1}{2X/Z_0}\right) Z_0 \\ -\dfrac{j}{Z_0}\left(\sin\phi + \dfrac{\cos\phi + 1}{2X/Z_0}\right) & \cos\phi - \dfrac{\sin\phi}{2X/Z_0} \end{bmatrix} \tag{12}$$

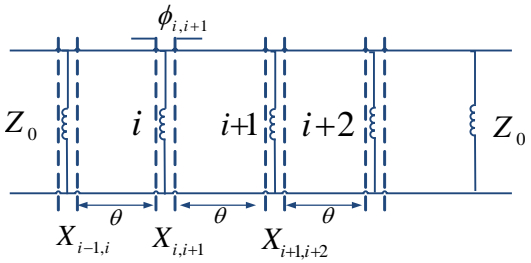

Figure 3. Section of shunt inductive H-plane waveguide BPF.

According to the equal relationship between formulae (11) and (12), formulae (13)–(15) can be obtained.

$$\phi = -\tan^{-1}\left(\frac{2X}{Z_0}\right) \tag{13}$$

$$K = Z_0 \tan\left(\frac{\phi}{2}\right) \tag{14}$$

$$\left|\frac{X}{Z_0}\right| = \frac{\dfrac{K}{Z_0}}{1-\left(\dfrac{K}{Z_0}\right)^2} \tag{15}$$

K and X have approximately the same linear frequency dependency. Since ϕ is small even for fairly broad-band filters,

$$\left(\frac{K}{Z_0}\right)^2 = \left(\tan\left(\frac{\phi}{2}\right)\right)^2 \ll 1 \tag{16}$$

and then (15) gives

$$\frac{X}{Z_0} \simeq \frac{K}{Z_0} \tag{17}$$

In the case of actual manufacture of thin diaphragm, the round chamfer is unavoidable, and the cutaway view is shown in Fig. 4. b, t, L_n and R are the width of the waveguide, thickness of the diaphragm, length of the nth resonator and radius of round corner chamfer respectively. The equivalent circuit of diaphragm is shown in Fig. 5. Fig. 5(a) shows the equivalent circuit of diaphragm without chamfer, and Fig. 5(b) shows the equivalent circuit of diaphragm with round chamfer. The length of resonator and size of inductive diaphragm with round chamfer can be obtained with impedance transformation. X_{sj} is the added reactance slope parameters owing to the round chamfer. Therefore, we have formulae (18) and (19) from formulae (13) and (14). Finally, the reactance slope parameters of the series resonators $X'_{j,j+1}$ can be obtained from formula (20), which is deduced from formulae (18) and (19).

$$\phi = -\tan^{-1}\left(\frac{2X + X_S}{Z_0}\right) \tag{18}$$

$$K = Z_0 \tan\left|\left(\frac{\phi}{2} + \arctan X_S\right)\right| \tag{19}$$

$$\frac{X'_{j,j+1}}{Z_0} = \frac{\dfrac{K_{j,j+1}}{Z_0}}{1-\left(\dfrac{K_{j,j+1}}{Z_0}\right)^2} = \tan\left|-\frac{\tan^{-1}\left(\dfrac{2X_{j,j+1}+X_{Sj}}{Z_0}\right)}{2} + \tan^{-1} X_{sj}\right| \tag{20}$$

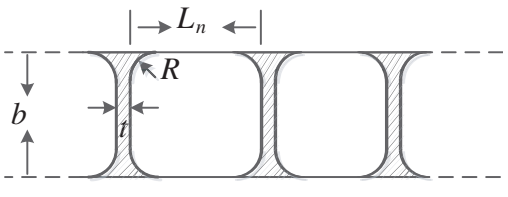

Figure 4. The structure of diaphragm with chamfer.

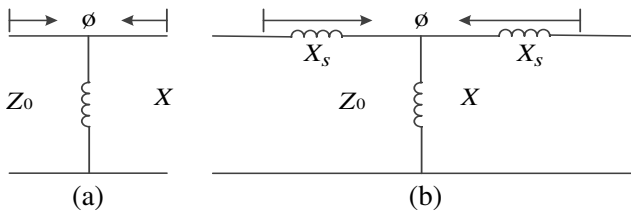

Figure 5. The equivalent circuit of impedance converter, (a) the equivalent circuit of diaphragm without chamfer, (b) the equivalent circuit of diaphragm with chamfer.

From Fig. 5(b), the length $\phi/2$ of both sides of the shunt inductance and chamfer should be merged into the electrical length of adjacent resonators. So the actual electrical length of the resonator is expressed in formula (21).

$$\begin{aligned}\theta_j &= \pi - \frac{1}{2}\left[\tan^{-1}\left(\frac{2X'_{j-1,j}}{Z_0}\right) + \tan^{-1}\left(\frac{2X'_{j,j+1}}{Z_0}\right)\right] \\ &= \pi - \frac{1}{2}\left[\begin{array}{l}\tan^{-1}\left(2\tan\left|-\dfrac{\tan^{-1}\left(\dfrac{2X_{j-1,j}+X_{Sj}}{Z_0}\right)}{2} + \tan^{-1}X_{Sj}\right|\right) \\ +\tan^{-1}\left(2\tan\left|-\dfrac{\tan^{-1}\left(\dfrac{2X_{j,j+1}+X_{Sj}}{Z_0}\right)}{2} + \tan^{-1}X_{Sj}\right|\right)\end{array}\right]\end{aligned} \tag{21}$$

λ_0 is the working wavelength of BPF and L_j the length of the resonator of BPF. Formula (22) expresses the inverse ratio of the center frequency and the length of the resonator of BPF.

$$L_j = \theta_j\lambda_0/2\pi \tag{22}$$

Formulae (18) to (22) show that the chamfer leads to the center frequency shifting of waveguide BPF. Based on formula (21) the relationship between the actual electrical length and the chamfer reactance slope of a H-plane waveguide BPF with 26 GHz center frequency is shown in Fig. 6. When the reactance slope of chamfer X_s decreases, the actual electrical length of resonators decreases. As shown in Fig. 6, the center frequency of H-plane waveguide BPF will shift toward higher frequency. When the chamfer radius increases, it will decrease the actual length of resonators and lead to the center frequency shift toward higher frequency. The equivalent circuit values of the 26 GHz waveguide BPF can be derived and given in Table 1.

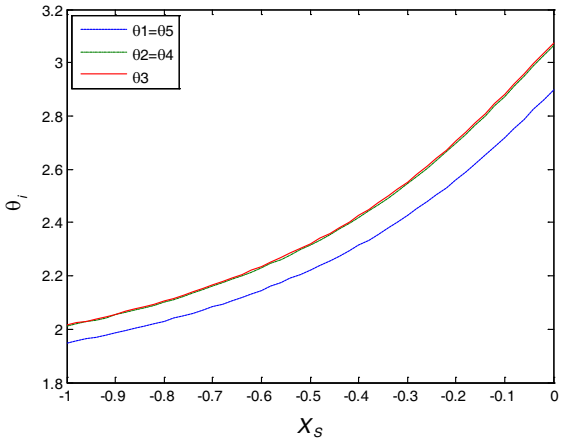

Figure 6. The relation between the actual electrical length and the reactance slope of chamfer.

In order to show the effects of chamfer, 5-order H-plane waveguide BPFs with different center frequencies and different 3 dB BWs are shown in Fig. 7 and Fig. 8. Figs. 7(a) to (d) show the filters with center frequencies 18 GHz, 26 GHz, 34 GHz and 42 GHz, and that the frequency shifting increases with BW when the chamfer radius changes from 0.1 mm to 0.7 mm.

Figures 8(a) to (e) show 3 dB BW with different center frequencies, 18 GHz, 26 GHz, 34 GHz and 42 GHz, respectively. Fig. 8 shows that frequency shifting increases with the increasing center frequency and chamfer radius. Based on Fig. 8(a)–Fig. 8(e), the value of frequency shifting increases with BW. These results are in good agreement with formulae (18)–(21).

Table 1. The equivalent circuit values of the 26 GHz waveguide BPF of Fig. 5(b).

Parameters of low-pass prototype filter	value	reactance slope	value (Ω)	reactance slope of chamfer	value (Ω)
$g_0 = g_6$	1	$X_{0,1} = X_{5,6}$	0.2037	$X_{s1} = X_{s5}$	−0.133
$g_1 = g_5$	1.3394	$X_{1,2} = X_{4,5}$	0.0415	$X_{s2} = X_{s4}$	−0.058
$g_2 = g_4$	1.337	$X_{2,3} = X_{3,4}$	0.03266	X_{s3}	−0.047
g_3	2.166				

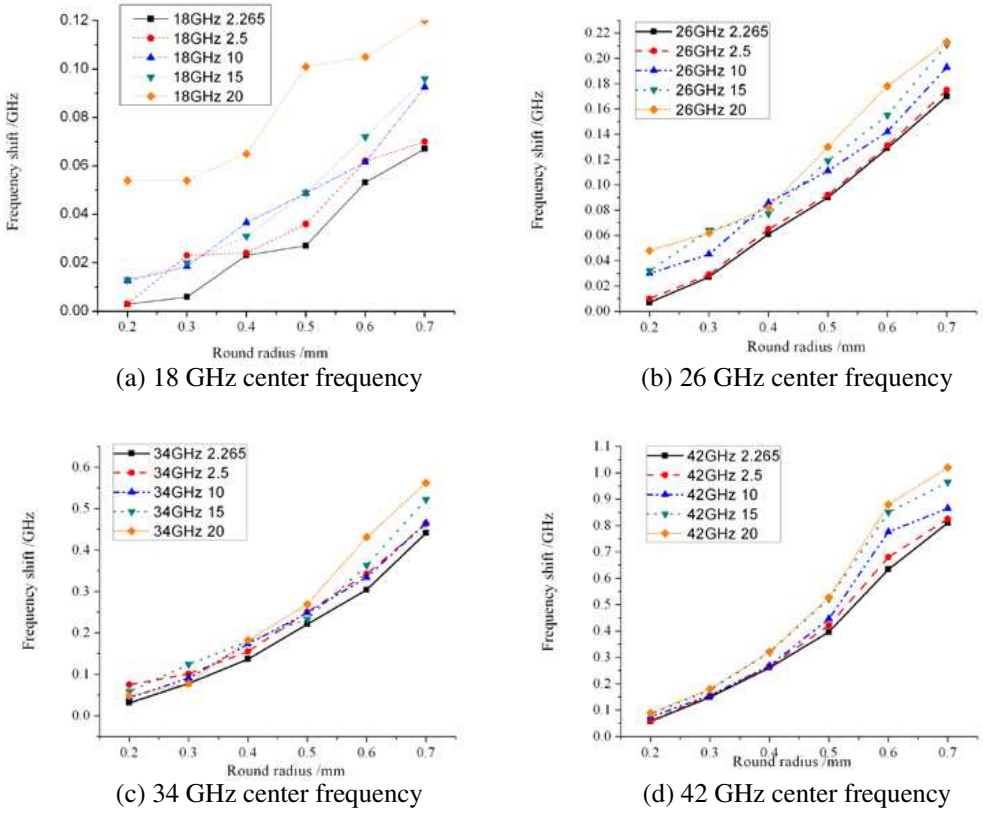

(a) 18 GHz center frequency (b) 26 GHz center frequency

(c) 34 GHz center frequency (d) 42 GHz center frequency

Figure 7. The frequency shifting with different center frequencies, (a) 18 GHz center frequency, (b) 26 GHz center frequency, (c) 34 GHz center frequency, (d) 42 GHz center frequency

3. MEASUREMENT RESULTS

Due to the center frequency shifting of the BPF, we need to consider the effects of the round chamfer in order to precisely design the filter response. With the help of formulae (18)–(22), two 5-order H-plane waveguide BPFs are designed with exact center frequencies of 26 GHz and 34 GHz. Their pass-bands are all 0.5 GHz with Chebyshev response. The insertion loss of two H-plane waveguide BPFs are less than 0.5 dB, and their image rejections are greater than 60 dB. Measurements were carried out at a Vector Network Analyser Agilent N5225A. All measurement results are calibrated by TRL [8, 16] method for de-embedding. For the tuning of the wave guide BPF, the stress of the two halves of the filter can be adjusted just as in Fig. 9 and Fig. 10. Fig. 10(a) shows half of the BPF, and Fig. 10(b) shows the manufactured BPFS.

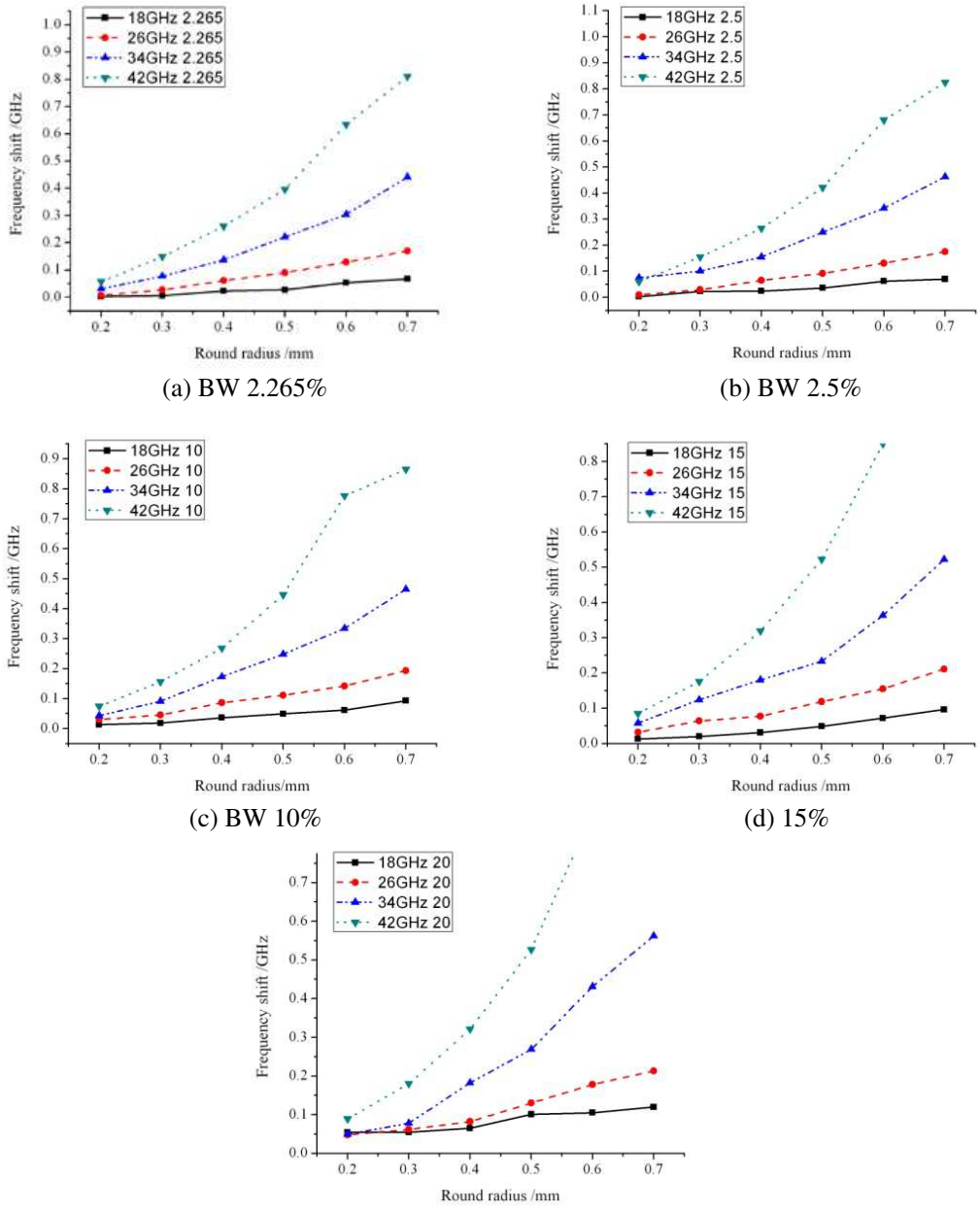

Figure 8. The frequency shifting with the same 3 dB BW, (a) BW 2.265%, (b) BW 2.5%, (c) BW 10%, (d) BW 15%, (e) BW 20%.

According to the above theoretical analysis of waveguide filter equivalent circuit, we can obtain the length of cavities and width of diaphragm shown in Table 1.

The filter was designed using direct coupled cavity theory [11] with modified formulae (18)–(22). The physical dimensions were obtained and listed in Table 2. After considering the round chamfer, L_1 to L_5 of each resonator of 26 GHz BPF and 34 GHz BPFs are increased to compensate the frequency shifting toward higher frequency, because the length of resonator is inversely proportional to its resonate frequency. The lengths of tune 1 to tune 5 of 26 GHz BPF and 34 GHz BPF are increased accordingly.

According to the modified dimensions in Table 2, the 26 GHz and 34 GHz filters are manufactured.

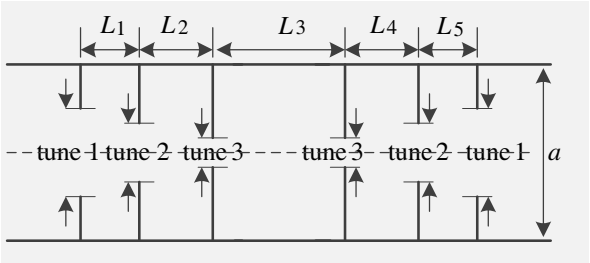

Figure 9. Top view of H-plane waveguide BPF.

(a) The half of H-plane waveguide BPF (b) The samples of the BPF

Figure 10. Photograph of the H-plane BPF, (a) the half of the BPF, (b) samples of the BPF.

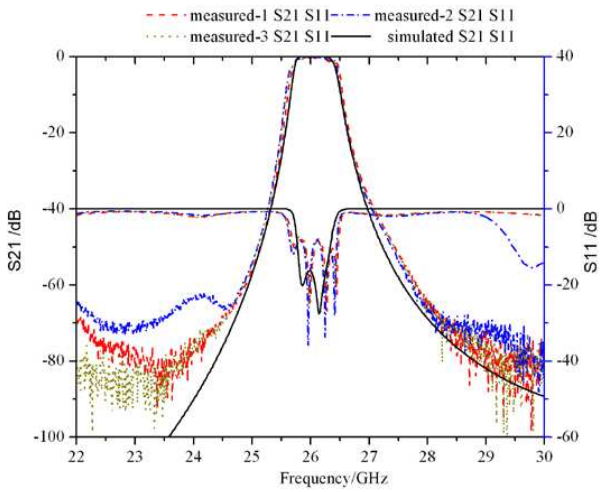

(a) 26 GHz BPF

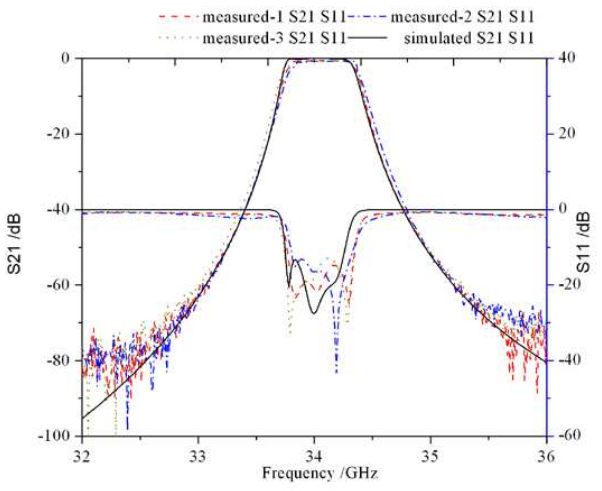

(b) 34 GHz BPF

Figure 11. Measurement results and simulation results of BPF, (a) 26 GHz BPF, (b) 34 GHz BPF.

Good agreement between measurement and simulation results can be seen from Fig. 11(a) and Fig. 11(b). Their 3 dB BW are 0.65 GHz and 0.77 GHz, respectively, and their 0.5 GHz pass-bands can be achieved. The 60 dB imaging rejections for the two H-plane waveguide BPFs are shown, and insertion loss is less than 0.5 dB. More details of the measured results of the fabricated filters are listed in Table 3. The results show excellent match in terms of reproducibility between two manufactured samples.

Table 2. Comparison of the dimensions of H-plane waveguide BPFs used modified formula.

Name	Original Size (mm)/26 GHz	Modified Size (mm)/26 GHz	Original Size (mm)/34 GHz	Modified Size (mm)/26 GHz
$L_1 = L_5$	6.65	6.69	4.94	5.08
$L_2 = L_4$	7.39	7.41	5.41	5.50
L_3	7.44	7.49	5.44	5.54
Tune 1	3.95	3.99	2.81	2.83
Tune 2	2.27	2.29	1.47	1.51
Tune 3	1.94	1.96	1.27	1.31

Table 3. Measurement results of H-plane waveguide BPFs used modified formula.

Name	Modified/26 GHz			Modified/34 GHz		
	I	II	III	I	II	III
3 dB BW	0.65	0.655	0.66	0.77	0.774	0.78
Insertion loss/dB	0.5	0.45	0.47	0.41	0.40	0.38
Return loss/dB	−22	−23	−22	−25	−27	−28
Ripple/dB	0.5	0.45	0.44	0.3	0.39	0.31
Imaging	−66	−68	−80	−72	−73	−74
suppression 1/dB	(22 GHz)	(22 GHz)	(22 GHz)	(30 GHz)	(30 GHz)	(30 GHz)
Imaging	−68	−70	−73	−72	−72	−75
suppression 2/dB	(28 GHz)	(28 GHz)	(28 GHz)	(38 GHz)	(38 GHz)	(38 GHz)

4. CONCLUSIONS

In this paper, a new design method of H-plane waveguide BPF is presented. This method considers the unavoidable chamfer during manufacturing, which will lead to center frequency shifting if uncorrected. Based on the physical inductance model of BPF considering chamfer, a modified formula is presented which will compensate the effect of frequency shifting.

The actual measurement results show that the center frequency is in good agreement with the modified formula and proves the validity of the new design method.

The method considering manufacturing chamfer is nontrivial in practice, and the modified formula provides theoretical basis for future manufacturing H-plane waveguide BPF.

REFERENCES

1. Sinclair, G. N., R. N. Anderton, and R. Appleby, "Outdoor passive millimeter wave security screening," *2001 IEEE 35th International Carnahan on Security Technology*, 172–179, 2001.
2. Wang, N.-N., J.-H. Qiu, and W.-B. Deng, "Development status of millimeter wave imaging systems for concealed detection," *Infrared Technology*, Vol. 31, No. 3, 129–135, China, 2009.
3. Nanzer, J. A. and R. L. Rogers, "Human presence detection using millimetre-wave radiometry," *IEEE Trans. Microw. Theory & Tech.*, Vol. 55, No. 12, 2727–2733, 2007.
4. Xue, Y., J. Miao, G. Wan, A. Hu, and F. Zhao, "Prototype development of an 8 mm band 2-dimensional aperture synthesis radiometer," *2008 International Geoscience and Remote Sensing Symposium*, Boston, 2008.
5. Zheng, C., X. Yao, A. Hu, and J. Miao, "A passive millimeter-wave imager used for concealed weapon detection," *Progress In Electromagnetics Research B*, Vol. 46, 279–297, 2013.

6. Zheng, C., X. Yao, A. Hu, and J. Miao, "Statistical power measurement unit for an 8 mm-band two dimensional synthetic aperture interferometric radiometer BHU-2D," *Progress In Electromagnetics Research M*, Vol. 27, 119–128, 2012.
7. Yang, B.-H., Z.-P. Li, T.-F. Yu, et al., "Design of receiver used for passive millimeter waveimaging system," *TELKOMNIKA*, Vol. 12, No. 1, 98–105, 2014.
8. Li, L., K. Wu, and P. Russer, "On the thru-reflect-line (TRL) numerical calibration and error analysis for parameter extraction of circuit model," *International Journal of RF and Microwave Computer-Aided Engineering*, Vol. 16, No. 5, 470–482, 2006.
9. Zhang, J., Z. Li, C. Zheng, X. Yao, B. Yang, and J. Miao, "Local oscillator uncorrelated phase noiseanalysis for millimeter-wave passive imager BHU-2D frequency synthesizer," *Progress In Electromagnetics Research B*, Vol. 54, 89–106, 2013.
10. Usher, J. and W. J. R. Hoefer, "Tunable microwave and millimeter-wave band-pass filter," *IEEE Trans. Microwave Theory and Techniques*, Vol. 39, 643–653, Apr. 1991.
11. Zhao, M., Y. Fan, and Y. Zhang, "A W-band low loss E-plane type waveguide band-pass filter," *IEEE 2007 International Symposium on Microwave, Antenna, Propagation and EMC Technologies for Wireless Communications*, 355–357, 2007.
12. Zhao, M. and Y. Fan, "A Ka band low loss wideband E-plane waveguide filter," *Proceedings of 2011 4th IEEE International Symposium on Microwave, Antenna, Propagation and EMC Technologies for Wireless Communications, MAPE 2011*, 802–804, 2011.
13. Lorente, J. A., C. Ernst, and A. A. Melcon, "Rigorous derivation of lossy equivalent circuit for narrowband waveguide direct-coupled-cavity filters," *IET Microw. Antennas Propag.*, Vol. 7, No. 4, 251–258, 2013.
14. Bahl, I. and P. Bhartia, *Microwave Solid State Circuit Design*, John Wiley & Sons Inc., 2003.
15. Levy, R., "Theory of direct-coupled-cavity filters," *IEE Transactions on Microwave Theory and Techniques*, Vol. 15, No. 6, 340–347, 1967.
16. Yang, B.-H., G. Mehdi, A. Hu, et al., "The round-ended design and measurement of all symmetric edge-coupledbandpass filter," *Progress In Electromagnetics Research C*, Vol. 136, 17–27, 2013.